Journal of Environmental Health Science and Engineering (2022) 20:915–930
https://doi.org/10.1007/s40201-022-00831-0

RESEARCH ARTICLE

Facile encapsulation of nano zero-valent iron with calcium carbonate: synthesis, characterization and application for iron remediation

Jismy Antony[1] · V. Meera[1] · Vinod P. Raphael[2] · P. Vinod[3]

Received: 3 June 2022 / Accepted: 16 August 2022 / Published online: 14 September 2022

Abstract In this study, $CaCO_3$ was used as a modifier for nano zero-valent iron (nZVI) surface to prevent rapid aggregation and effectively utilized for iron remediation from aqueous solution. Surface chemistry and morphology of $CaCO_3$ encapsulated nZVI ($CaCO_3$–nZVI) before and after treatment of contaminant iron solution were characterized by scanning electron microscopy–energy dispersive X-ray (SEM–EDX), X-ray diffraction (XRD), transmission electron microscopy (TEM), Fourier transform infrared spectroscopy (FTIR), and X-ray photoelectron spectroscopy (XPS). The mechanisms of surface modification as well as iron remediation were well depicted with the help of these characterisation tools. Iron removal efficacy of 96.4% was achieved with 0.25 g/L adsorbent dose for an influent iron of 0.5 mg/L at pH 10 after a 3 h treatment process. When the influent concentration was increased to 10 mg/L, the removal capacity decreased to 92.1%. The study demonstrates that $CaCO_3$ and nZVI in the encapsulated nanoparticle have a significant synergistic effect. The pseudo-second- order reaction kinetics and Freundlich isotherm model correctly portrayed the experimental data for iron removal by $CaCO_3$–nZVI. The $CaCO_3$–nZVI is a viable option for iron removal from various aqueous media due to its facile preparation, high iron removal capability, and reusability.

Keywords $CaCO_3$-nZVI · Iron removal · Adsorption · Surface modification · XPS · BET

*Corresponding Author-Meera V., Email: vmeera@gectcr.ac.in 9,895,160,573.

Graphical abstract.

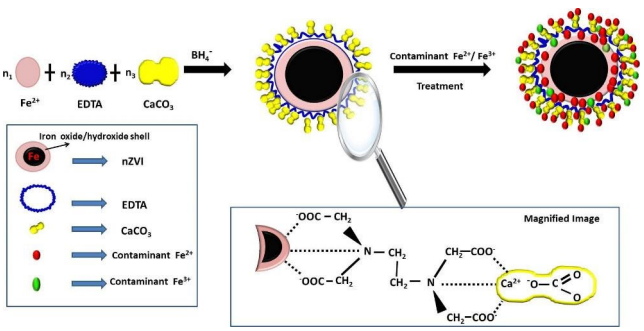

Introduction

The current challenges in the world-wide water situation demand novel advanced technologies to guarantee the drinking water quality and to minimise global water pollution. Nowadays, the ground/surface water sources are mainly contaminated by heavy metals, emerging micro-contaminants, fertilizers, detergents, pesticides, and so forth [1]. Currently, heavy metals are the major concern in environmental and industrial research [2]. Heavy metals can be

✉ V. Meera
vmeera@gectcr.ac.in

1 Department of Civil Engineering, Government Engineering College Thrissur, APJ Abdul Kalam Technological University, 695016 Thiruvananthapuram, India

2 Department of Chemistry, Government Engineering College Thrissur, APJ Abdul Kalam Technological University, 695016 Thiruvananthapuram, India

3 Department of Civil Engineering, Marian Engineering College Thiruvananthapuram, APJ Abdul Kalam Technological University, 695016 Thiruvananthapuram, India

found in trace levels in natural water bodies [3, 4]. The environment requires a suitable concentration of these metals for its proper metabolism. As rain water permeates through the rocks, it dissolves trace amounts of metals and naturally enters into water bodies [5]. Iron is one of these metals that can be found in rocks and soil. It ranks second in earth's crust and fourth among the foremost rich elements on earth [6]. Even though iron plays a major role as a vital mineral nutrient, excessive iron in water is a problematic issue in making clean drinking water. Iron contamination occurs in water resources due to the leaching from rocks, industrial dumping, corrosion of iron pipes etc.

Iron in water supplies and drinking water creates aesthetic-health issues and clogging problems as well as corrosion effects in water distribution systems [7, 8]. Overexposure to iron, on the other hand, can result in health problems such as hyperkeratosis, cardiovascular disease, diabetes, liver, kidney, neurological and respiratory disorders[9]. Iron can cause retinitis, conjunctivitis and choroiditis, if it comes into contact with and persists in the tissues[10]. Iron overload can impair hematopoiesis by destroying microenvironment and progenitor cells for the formation of cellular blood components. Hemochromatosis is a condition in which the body's iron levels are too high, causing damage to various organs [6]. Too much iron can be harmful to the gastrointestinal system. Iron toxicity causes stomach pain, diarrhoea and vomiting. Over time, iron can accumulate in the organs, causing catastrophic damage to brain or liver [11].

Iron contamination is currently posing a serious threat to drinking water sources all over the world. The average groundwater iron level was reported as 1.422 mg/L, ranging from 0.134 to 5.2 mg/L among the household wells of Cambodia's rural Prey Veng province [12]. Excessive iron content was found in 17% of residential water supplies sampled in Pennsylvania, according to a state survey [13]. The iron content in groundwater of Tangail municipality, Bangladesh, was found to be 1.03–24.50 mg/L[14]. Iron was identified as the most common pollutant in a research carried out by the Central Water Commission (CWC) during 2014–2018, in India with 156 of the 442 sampled sites having iron concentration above the admissible limit [15]. Studies conducted in most places in Thiruvananthapuram, Kerala (a southern state of India), by the Kerala State Pollution Control Board, on the Kerala Water Authority's water supply quality, found higher iron values (1.02-1.47 mg/L) [16]. These reports of increasing iron contamination as well as the revised stringent standard for drinking water (permissible limit – 0.3 mg/L) demand more researches to develop stable and cost-effective methods/materials for the efficient removal of iron from water bodies.

Nano zero-valent iron (nZVI) has gained a lot of interest as a potential candidate for cleaning up various inorganic and organic pollutants [17, 18]. The presence of more reactive sites and large surface area [19, 20] provide high surface energy and reactivity for the nZVI. Thus it exhibits outstanding performance in removing priority water pollutants at low environmental and ecnomic costs [4]. nZVI was used to remove heavy metals from wastewater in a study by Oprackal et al. 2017, and observed a decrease of influent iron concentration which indicates the potential of nZVI for iron remediation [21]. In our previous work [7, 8], the capacity of nZVI has been explored and found that nZVI is capable of removing 70% iron with 0.5 g/L dose at pH 10 (optimum) from a sample having 0.5 mg/L influent iron. Even though nZVI exhibits significant iron removal, the characterization study shows high agglomeration due to the forces between each nanoparticle. These aggregations produce an adverse effect on the surface area; number of reactive sites and in turn its performance on the removal capacity.

The issues associated with the agglomeration behaviour of the nZVI can be addressed by the surface modification/immobilization of nZVI with agents such as clay minerals [22–26], surfactants [27–30] and polymers [31–33]. Recently, Calcium carbonate ($CaCO_3$) has piqued the interest of researchers due to its ease of modification and control in forming a specific structure [34, 35]. Moreover, it is a easily available natural resource and completely biodegradable as well as environmental friendly material [36]. $CaCO_3$ is particularly effective at removing heavy metal ions because of its excellent adsorption capacity and unique structural characteristics [37–39]. nZVI particles modified by $CaCO_3$ have been reported to increase their stability and dispersibility [35, 40]. However, there are no studies of encapsulating nZVI in calcium carbonate for iron remediation. The potential of calcium carbonate encapsulated zero-valent iron nanoparticle ($CaCO_3$-nZVI) for iron remediation was investigated in this work, and the removal mechanism was elucidated using various spectroscopic and microscopic analyses. The results of various operational parameters (nanoparticle dose, pH, influent iron content and process time) were interpreted using kinetic and isotherm models.

Materials and methods

Chemicals and instruments

Analytical grade reagents such as ferrous sulphate heptahydrate ($FeSO_4.7H_2O$), calcium carbonate ($CaCO_3$), ethylenediamine tetraacetic acid (EDTA), sodium borohydride ($NaBH_4$), ethanol (CH_3CH_2OH), ferric ammonium sulphate ($NH_4Fe(SO_4)_2.12H_2O$), ferrous ammonium sulphate ($(NH_4)_2Fe(SO_4)_2.6H_2O$), hydrochloric acid (HCl)

and sodium hydroxide (NaOH) were procured from Merck Millipore.

Ultrasonic homogeniser sonicator of 20 kHz frequency with 12 mm ultrasonic probe was used for dispersing $CaCO_3$ in ethanol. Remi R-12 M laboratory centrifuge and Palintest PTBH-7500 photometer were used for separation of nanoparticles and analysis of contaminant iron, respectively.

Synthesis of calcium carbonate encapsulated nano zero-valent iron ($CaCO_3$-nZVI)

The liquid-phase reduction process is used to synthesise both bare nZVI and $CaCO_3$-encapsulated nZVI.[24, 41]. $CaCO_3$-nZVI was synthesised by adding a certain amount of $CaCO_3$ to 150 mL of ethanol according to the desired $CaCO_3$/Fe ratio and 10 min of dispersion was given by an ultrasonic sonicator. The amount of $CaCO_3$ was varied as 0.17, 0.34, 0.51, and 0.68 g to obtain $CaCO_3$ to theoretical Fe ratios of 0.2, 0.4, 0.6, and 0.8, respectively. 4.17 g $FeSO_4.7H_2O$ (theoretical Fe content: 0.84 g) was dissolved in 150 mL distilled water and gently mixed with 100 mL 0.05 M EDTA solution. $CaCO_3$ suspension was added to a two-neck round bottom flask and blended with $FeSO_4.7H_2O$ and EDTA solution. Nitrogen purging removed the dissolved oxygen. Then 2.84 g $NaBH_4$ was dissolved in 100 mL distilled water and dropped into the flask while constantly shaking it. After introducing the entire reductant, the mixture was stirred again for 20 min. Centrifugation was used to collect the formed black nanoparticles, which were then washed three times with ethanol. The particles were oven-dried at 50^0 C before being stored in a tight container under normal conditions. The best composite was selected based on the iron removal capacity and employed for future studies.

Characterization studies

Transmission electron microscope (TEM, Jeol/JEM 2100) was employed to analyse the particle size, dispersity and morphology of both nZVI and $CaCO_3$-nZVI. Scanning electron microscopy (SEM) and energy dispersive X-ray spectroscopy (EDX) mapping were used to characterise the morphological properties and basic composition of fresh and used $CaCO_3$-nZVI.The instrument Carlz Zeiss Evo 18 was used for this analysis at different magnification.

N_2 adsorption-desorption isotherms were used to determine pore size, surface area and pore volume distribution using a Brunauer-–Emmett–Teller surface area analyser (Belsorp Max, MicrotracBelsorp, Japan). The interactive functional groups that participate in both modification and iron removal were identified using Fourier infrared (FTIR) analysis. Thermo Nicolet Avtar 370 model spectrometer was used to record FTIR spectrum in the transmission mode at room temperature using KBr pellets in the range 400–4000 cm^{-1}. The crystal structure of $CaCO_3$-nZVI was divulged by X-ray powder diffraction (XRD) patterns recorded on Bruker D8 diffractometer with a CuKα (λ = 1.54 Å) high-power source which operates at 40 kV/ 40 mA. X-ray photoelectron spectrophotometer (PHI 5000 Versa Probe II, ULVAC-PHI Inc.) having Al-Kα X-ray source was used to identify the elements and their respective valence states in fresh and used $CaCO_3$-nZVI.

Point of zero charge (pH_{pzc}) of $CaCO_3$-nZVI

Point of zero charge (pH_{pzc}) of $CaCO_3$-nZVI was determined in the 0.1 M KCl solution. The pH of KCl solution was varied from 2 to 12 using 1 N NaOH and 1 N HCl. The $CaCO_3$-nZVI particles were added to these solutions and a control was also employed without any nanoparticles. The initial pH of control and sample was measured immediately after thorough mixing and final pH was checked after 24 h. The graph was plotted between initial and final pH for both control as well as sample. The meeting point of these curves was denoted as the point of zero charge.

Batch experiments

A set of batch tests were conducted to investigate the iron remediation potential of $CaCO_3$-nZVI by using 200 mL iron solution with desired concentration at room temperature. As iron in surface water sources has different ferrous to ferric ratio, a Fe^{2+}/Fe^{3+} ratio of 2.5:0.5 [42] was selected for the simulated surface water in this study. Iron samples of desired concentration with Fe^{2+}/Fe^{3+} ratio of 2.5:0.5 were prepared by dilution and mixing of ferrous and ferric stock solutions. The modified nanoparticles with $CaCO_3$/Fe ratio of 0.6 were employed for all batch experiments as it showed highest removal capacity among the different ratios selected.

To study the effect of contact time on the iron uptake, 0.1 g/L $CaCO_3$-nZVI nanoparticles were added to 200 mL iron solution of 0.5 mg/L, at influent pH and agitated in an orbital shaker for a period of 24 h. The samples were withdrawn and analysed at 1 h, 2 h, 3 h, 6 h, 12 and 24 h reaction period. Pseudo-first- and pseudo-second-order kinetic models were used to analyse the results. The Chi-square test (χ^2) and regression coefficient (R^2) were also used to evaluate the goodness of fit.

In the next stage of experiment, the pH of the iron solution was adjusted to the values in the range of 5–12 using 1 N HCl and/or 1 N NaOH and the influence of pH was found by treating the 0.5 mg/L iron samples for 3 h (optimum) with 0.1 g/L of $CaCO_3$-nZVI particles.

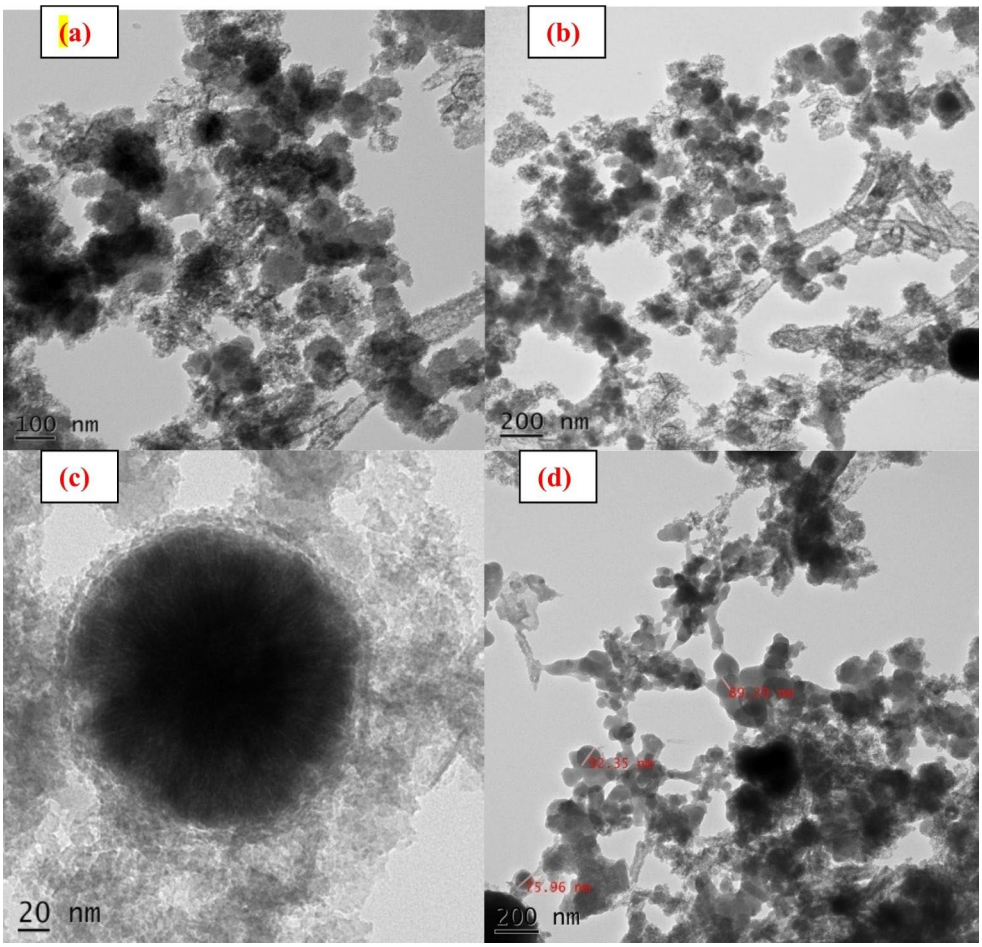

Fig. 1 **(a)-(d)** TEM images of $CaCO_3$-nZVI

Batch experiments were conducted at optimum pH and reaction period by adding different $CaCO_3$-nZVI dose (0.05-1 g/L) to samples having influent iron 0.5 mg/L to elucidate the role of amount of nanoparticle on iron removal.

Adsorption isotherms were obtained by treating iron solutions of different initial iron concentration (0.5–10 mg/L) for 3 h period at pH 10 using 0.25 g/L $CaCO_3$-nZVI. The utilized $CaCO_3$-nZVI nanoparticles were collected from the treatment system by centrifugation and their reuse capacity in fresh 0.5 mg/L iron solution at optimized conditions without any washing and desorption was investigated.

In all experiments, 10 mL sample was withdrawn at desired reaction time and allowed to settle for 20 min. The centrifugation as well as magnetic separation was used for the collected supernatant to separate $CaCO_3$-nZVI nanoparticles from the treated sample. Parallel experiments were conducted in all batches without adding the nanoparticles but otherwise under identical conditions (control). The total iron concentration in the treated sample and in control was analysed by using the Palintest PTBH-7500 photometer.

Results and discussion

Characterisation of $CaCO_3$ encapsulated nZVI

The particle size, shape and dispersion of bare and modified nZVI particles were characterised by TEM and depicted in Fig. 1a-d and Fig.S1a-d (shown in supplementary section), respectively. The $CaCO_3$-nZVI particles were well dispersed with spherical shape, while roughly spherical particles with large aggregation could be identified for bare nZVI. A clear and distinct outline is recognized for the modified particle (Fig. 1c) whereas it is hardly seen in the case of bare nZVI (Fig.S1c). The size of the $CaCO_3$-nZVI particles ranged from 75 to 89 nm, which was smaller than unmodified nZVI (80-99 nm). The surface modifier forms a layer on the nanoparticle surface which prevents the aggregation and in turn leads to the smaller size.$CaCO_3$ modification could reduce magnetic attraction and van der Waals forces between zero-valent iron nanoparticles, improving stability. Cheng et al. 2020 also reported similar images [40].

The chemical composition of freshly prepared $CaCO_3$-nZVI from the EDX analysis (Fig. 2) revealed the presence of Ca in addition to Fe, O and Na present in the

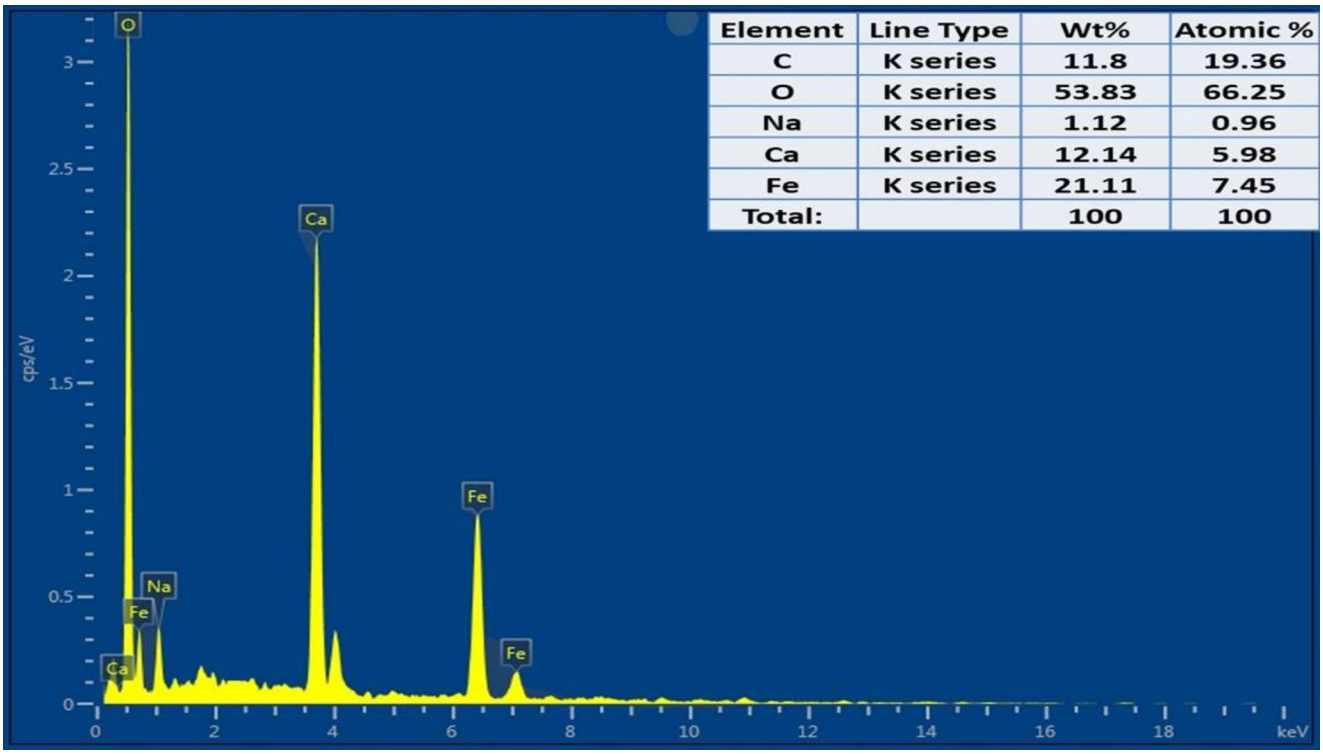

Fig. 2 EDX spectrum of $CaCO_3$-nZVI

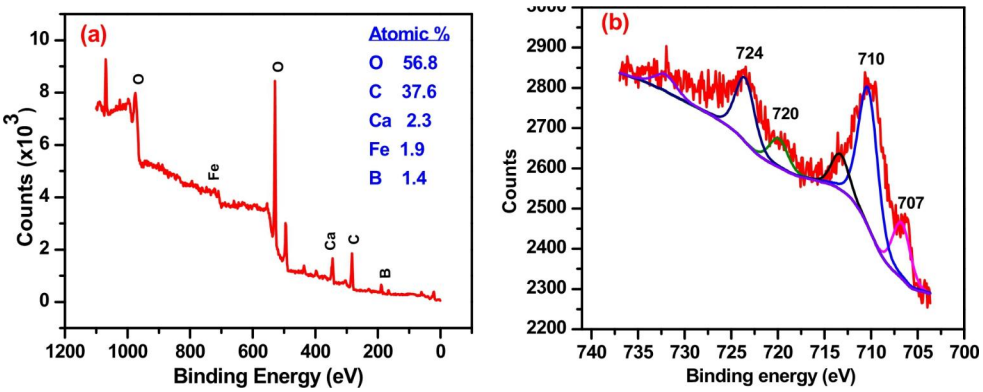

Fig. 3 **(a)** XPS surface spectrum of $CaCO_3$-nZVI and **(b)** Fe 2p spectrum of $CaCO_3$-nZVI

EDX spectrum of bare nZVI (Fig.S2).The XPS analysis of $CaCO_3$-nZVI surface (Fig. 3a) shows peaks at around 194, 284, 347, 531 and 710 eV revealing the presence of boron, carbon, calcium, oxygen and iron, respectively. Moreover, the diffraction peaks at 2θ angle of 29.38^0 and 47.5^0in XRD (Fig. 4) are the typical peaks of $CaCO_3$ [40]. The reflection peaks for the calcite crystals at 2θ angle of 29.4^0 and 47.5^0 were ascribed to (104) and (018) crystallographic plane [35], suggesting the successful encapsulation of nZVI by calcium carbonate in calcite phase.

The zero-valent state of iron in encapsulated nanoparticle is indicated by the peak at $2\theta = 44.6^0$ in XRD (Fig. 4) and the peak observed at 707 eV in the Fe 2p spectrum (Fig. 3b). The binding energies of $2p_{1/2}$ and $2p_{3/2}$ of iron oxide present in the nZVI surface can be attributed to the photoelectron peaks at 724 eV and 710 eV. The overlap of shakeup satellites of zero-valent iron ($2p_{1/2}$) and iron oxide ($2p_{3/2}$) resulted in the 720 eV shoulder [2]. These peaks are indicative of the oxide/hydroxide layer present around the core of zero-valent iron.

The surface area of both bare and modified nZVI was calculated using multi-point BET plots (Fig.S3a and S3b). The obtained surface area increases significantly from 20.12 m^2/g (bare-nZVI) to 26.67 m^2/g ($CaCO_3$-nZVI). The modified particles have a total pore volume of 0.115 cm^3/g and average pore diameter of 16.889 nm, whereas the unmodified nanoparticles have a total pore volume of 0.107 cm^3/g and average pore diameter of 17.45 nm. The increased surface area and pore volume imply that $CaCO_3$-nZVI may have a higher removal capacity than bare nZVI.

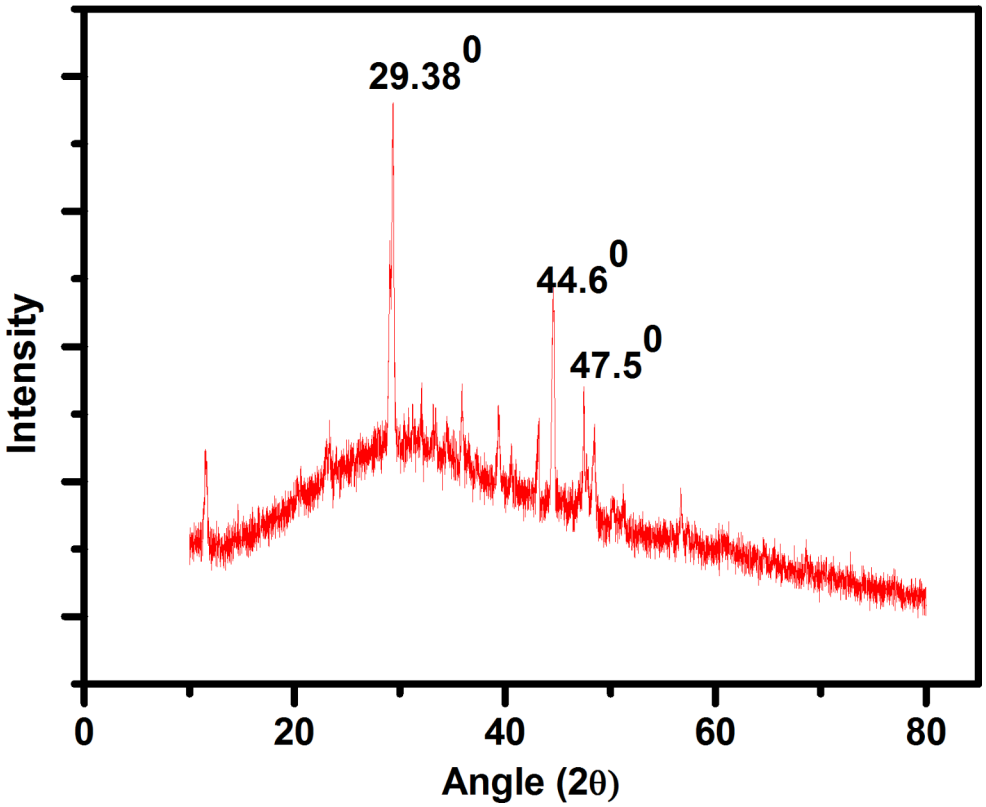

Fig. 4 XRD pattern of $CaCO_3$ encapsulated nZVI

Figure 5 shows the FTIR spectrum for nZVI and $CaCO_3$ encapsulated nZVI. The broad absorption band at 3410 – 3128 cm^{-1} is associated with O-H stretching vibration. The C-H bending vibrations are responsible for the band at 1383 cm^{-1}. The absorbance peak at 1107 cm^{-1} is correlated to C-O or C-O-C stretching vibrations [43]. These common peaks in the spectrum of both nZVI and $CaCO_3$-nZVI correspond to EDTA. The C = O stretching vibration present in EDTA as well as in $CaCO_3$ is illustrated by the absorbance peak at 1630 cm^{-1}. The comparison of the FTIR spectra of bare nZVI (Fig. 5a) and modified nZVI (Fig. 5b), reveals new peaks at 708, 873 and 1419 cm^{-1} for modified nZVI that correspond to in-plane bending, out-of-plane bending and asymmetrical stretching vibration peaks of O-C-O bonds present in $CaCO_3$ respectively [44]. Furthermore, the emergence of Ca-O bond stretching frequency at 534 cm^{-1} indicates the interaction between the carboxylate group of EDTA and calcium ions of $CaCO_3$ [45, 46]. The above results confirm that the modifier $CaCO_3$ was successfully loaded onto the nZVI surface.

Effect of influencing parameters on iron removal capacity

Effect of $CaCO_3$/Fe ratio in the $CaCO_3$-nZVI and contact time

The $CaCO_3$/Fe ratio in the modified nanoparticle as well as the contact time play a significant role in the contaminant iron removal efficiency, as shown in Fig. 6a. The adsorption performance of $CaCO_3$-nZVI improved when the $CaCO_3$/Fe ratio increased from 0.2 to 0.6, and $CaCO_3$-nZVI with a ratio of 0.6 showed the maximum removal efficiency of 78.6% at pH 6.85 with a 0.1 g/L dose. The modification of nanoparticles by $CaCO_3$ results in increased dispersion of sorbents. However, when the ratio was increased to 0.8, the removal efficiency decreased to 70%. This might be due to the fact that $CaCO_3$ content beyond optimum, occupies the reactive sites on the modified particle, hindering the adsorption of iron. The results also indicated that adsorption was rapid in the first few hours, with the highest removal efficiency at the end of three hours. There was no further increment in removal efficiency observed beyond 3 h and reaction rate reached the equilibrium condition. This fast adsorption rate indicates that large numbers of vacant sites are readily accessible for contaminant iron at the initial stage. The adsorption of contaminant iron to the vacant sites of $CaCO_3$-nZVI becomes difficult after a certain time due to

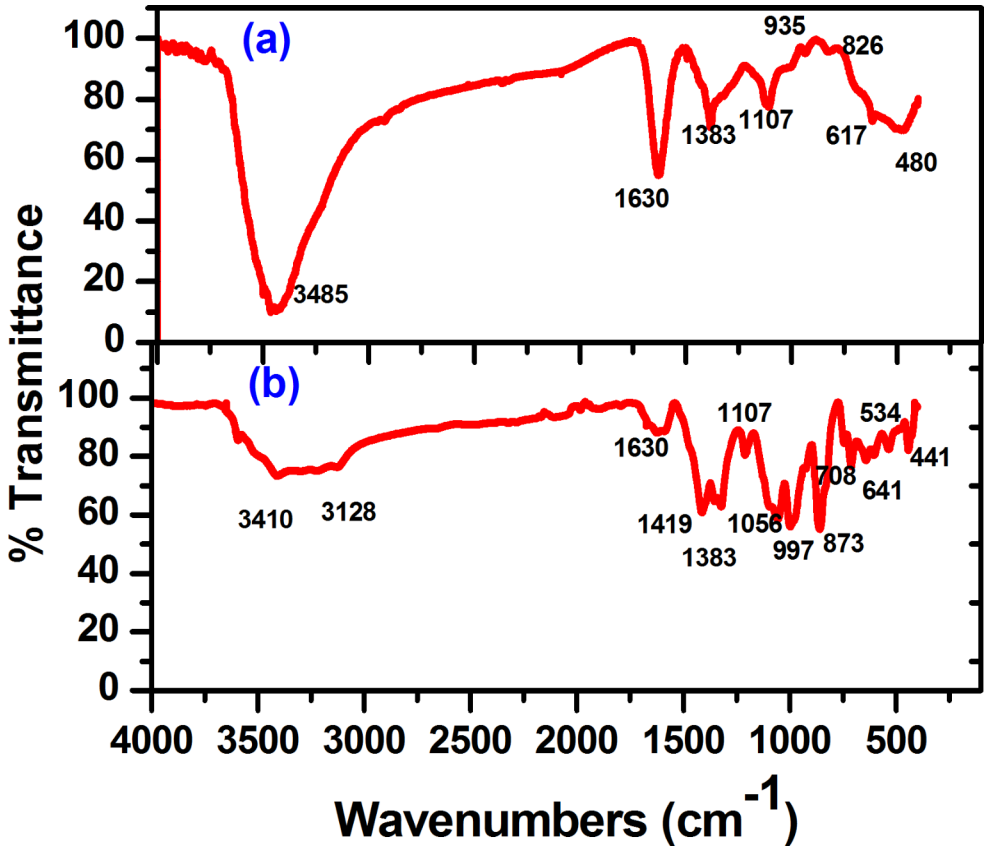

Fig. 5 FTIR spectrum of **(a)** nZVI and **(b)** $CaCO_3$ -nZVI

the repulsive forces between iron ions on the sorbent surface and in the solution.

Effect of pH

The pH of the solution affects both the metal chemistry and the surface charge of the $CaCO_3$-nZVI, making it an important factor in heavy metal removal. The adsorption performance of $CaCO_3$-nZVI (0.1 g/L) in 0.5 mg/L iron solution was monitored at different pH (5–12) for 3 h period (optimum) and is shown in Fig. 6b. At pH 10, the maximum removal efficiency of 88.4% was obtained. The lower removal efficiency in the acidic range is due to competition for vacant sites by H^+ ions and contaminant iron ions. The obtained point of zero charge for $CaCO_3$-nZVI was 9.21 (Fig.S4), implying that at pH > pHpzc, the sorbent surface will become negatively charged and enhance contaminant iron adsorption.

Effect of $CaCO_3$-nZVI dosage and influent iron concentration

The dosage of $CaCO_3$-nZVI is an important parameter in determining its uptake capacity for a given initial contaminant iron concentration. So, to elucidate the role of modified nanoparticle dose on the iron removal efficiency, 0.05-1 g/L $CaCO_3$-nZVI were used for treating the iron samples at optimum pH of 10. The involvement of influent iron concentration was investigated by varying the concentration for each $CaCO_3$- nZVI dose from 0.5 mg/L to 10 mg/L. Figure 6c depicts the results. The maximum iron removal was 96.2% at 0.25 g/L for 0.5 mg/L influent iron concentration, resulting in a final concentration of 0.018 mg/L, well below the acceptable limit for potable water. The optimum $CaCO_3$-nZVI dose for 10 mg/L influent iron sample was found to be 1 g/L and an iron removal efficiency of 92.1% was obtained at pH 10 and contact time 3 h.

The high removal efficiency at lower initial concentration for a given nanoparticle dose can be attributed to the high ratio of available active sites on the $CaCO_3$-nZVI surface to the influent iron concentration. As influent concentration rises, the availability of sorption active sites decreases, resulting in lower removal efficiency.

For a given influent iron concentration, an increase in $CaCO_3$-nZVI amount resulted in enhanced iron adsorption due to the availability of additional sites. The addition of $CaCO_3$-nZVI over the optimal dose for a given concentration, on the other hand, did not appreciably boost adsorption. As adsorbent dosage increases, the probability of collision between nanoparticles increases, causing particle aggregation, thereby the diffusion path length gets increased. This reduce the total surface area and iron adsorption rate [47].

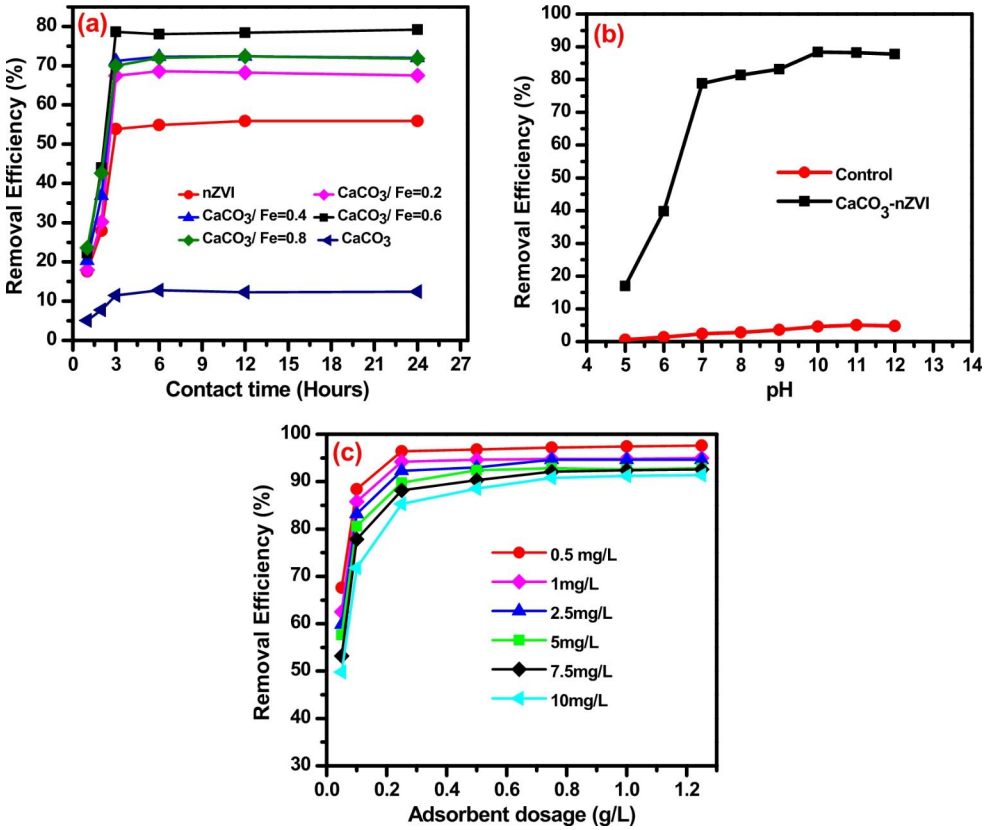

Fig. 6 Iron removal efficiency of $CaCO_3$-nZVI with varying **(a)** $CaCO_3$/Fe ratio in the $CaCO_3$-nZVI and contact time [pH = 6.85, dosage = 0.1 g/L, influent iron = 0.5 mg/L] **(b)** pH [$CaCO_3$/Fe ratio = 0.6, contact time = 3 h, dosage = 0.1 g/L, influent iron = 0.5 mg/L] **(c)** Influent iron concentration and adsorbent dosage [$CaCO_3$/Fe ratio = 0.6, contact time = 3 h, pH10]

For an influent iron concentration of 0.5 mg/L, the iron removal efficiency of $CaCO_3$-nZVI was 96.4%, while that for bare nZVI (contact time- 3 h, pH- 10, dosage-0.5 g/L) and $CaCO_3$ (contact time-3 h, pH- 10, dosage-0.5 g/L) were 70% and 23.8% respectively. The synergistic effect of modified particles in iron remediation is illustrated in Fig. 7.

Reusability of $CaCO_3$-nZVI

The easy recovery of the adsorbent from the treatment system and its reusing capacity make the technique more environment-friendly and economical. The $CaCO_3$-nZVI was recovered from the system by using centrifugation and reused without washing and desorption. The reusability performance of $CaCO_3$-nZVI in treatment of fresh iron sample of 0.5 mg/L concentration is illustrated in Fig. 8. The adsorbent possessed iron removal efficacy of 62.2% even after the 3rd cycle treatment. Depletion of active sites and effective surface led to the reduction of removal efficiency with each reuse.

Iron removal mechanism of $CaCO_3$-nZVI

Iron nanoparticles have a core-shell structure, with the core being Fe^0 and the shell being iron oxides/hydroxides [2]. Heavy metal removal from an aqueous system by nZVI is accomplished primarily through two distinct mechanisms. This includes (i) electron donation by the active core of nZVI to the heavy metal ions (redox process) and (ii) metal ion adsorption on the outer shell of nanoparticles (surface complexation). The first mechanism is used by nZVI to remove heavy metal ions whose standard reduction potential is less negative than the Fe potential. During this process, electrons are transferred from the outer oxide layer of nZVI to the metal ions in the solution, causing the inner core of nZVI to oxidise. The chance for the first mechanism to remove iron ions can be completely ruled out due to the same redox behaviour of the nanoparticles and the metal ions present in the aqueous medium. After treatment of $CaCO_3$-nZVI with the iron solution, the inner core of the nanoparticles remain intact as evident from the Fe^0 peaks ($2\theta = 44.6^0$) in XRD (Fig. 9) as well as in XPS (Fig. 10). These analyses clearly establish the mechanism of iron remediation by $CaCO_3$-nZVI as adsorption.

As represented in Figs. 10 and 11, increased atomic percentage of iron in XPS (1.9–14%) and the escalated weight% of iron in EDX (21.11–57.7%) confirmed the uptake of iron. The sorption of iron can be again validated by the emergence of small peaks corresponding to Fe3s and Fe3p around 90 eV in XPS as well as new 2θ peaks at 25.91^0, 35.99^0 and 57.42^0 which correspond to oxides of iron viz. Fe_2O_3 and Fe_3O_4. The iron adsorption on $CaCO_3$-nZVI is

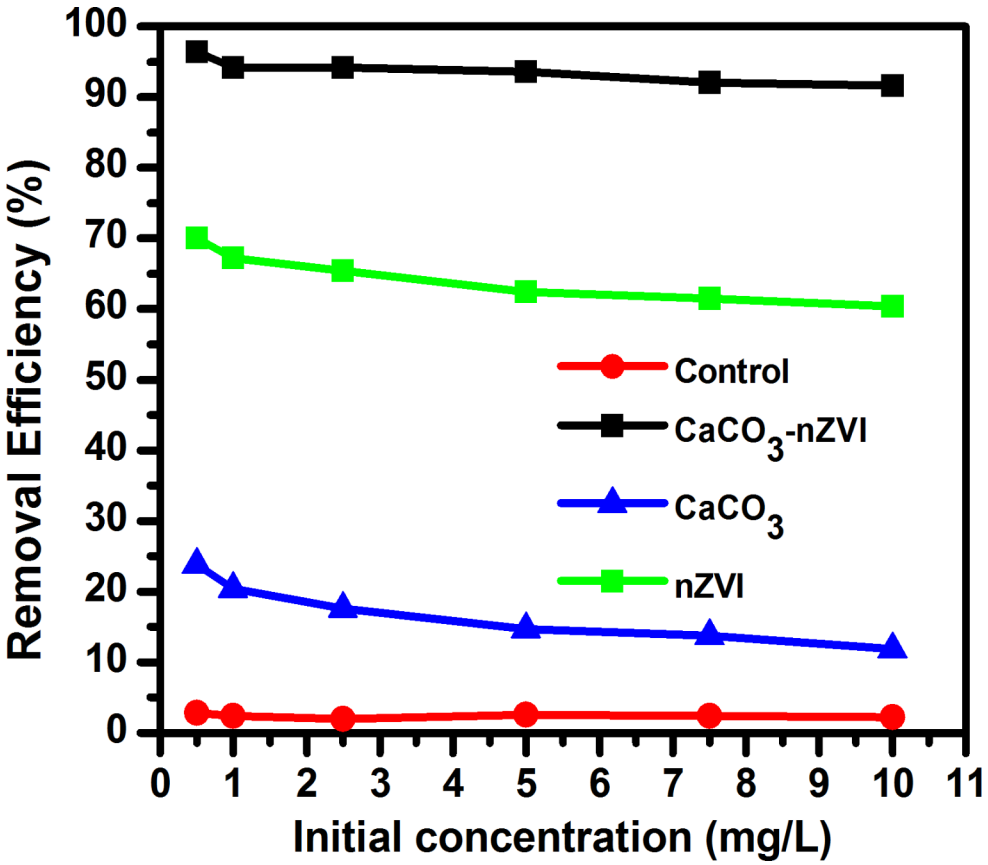

Fig. 7 Comparison of iron removal efficiency of $CaCO_3$, nZVI with $CaCO_3$-nZVI

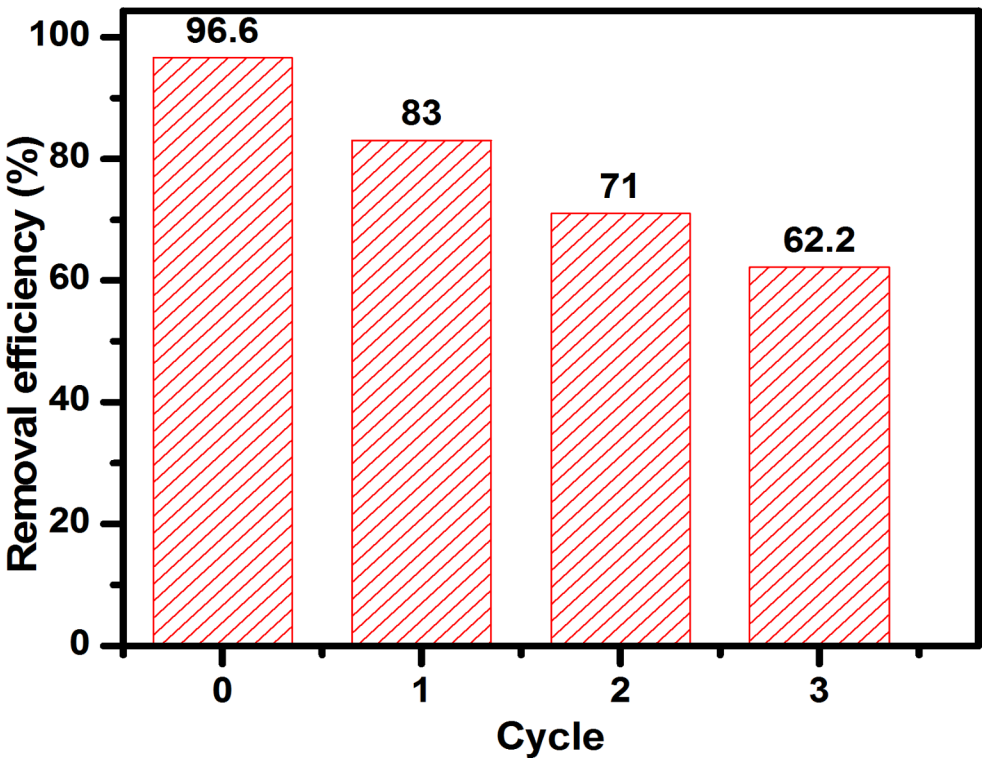

Fig. 8 Reusability of $CaCO_3$- nZVI

proposed to occur in the following ways in light of FTIR spectrum of nanoparticle (Fig. 12) after treatment:

1) The broad absorption band at 3410 – 3128 cm^{-1} corresponding to O-H stretching vibration is shifted to

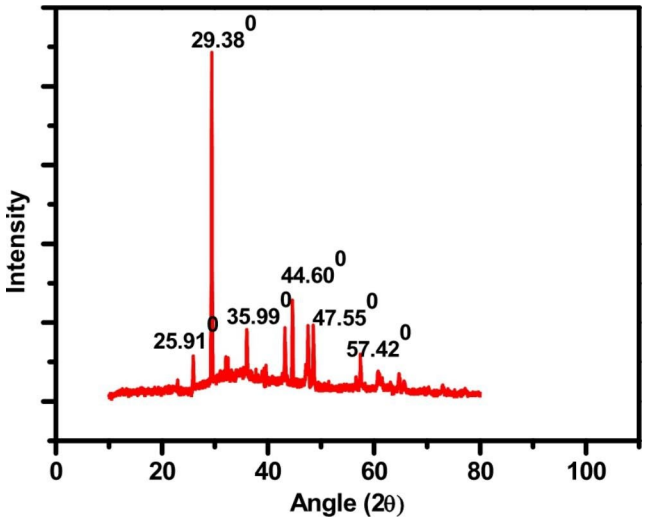

Fig. 9 XRD pattern of $CaCO_3$-nZVI after treatment

3360 cm^{-1} showing the possibility of contaminant iron adsorption on iron oxide/hydroxide shell.

2) The absorption band at 1630 cm^{-1} before treatment is shifted to 1618 cm^{-1} after treatment. This peak is attributed to the C = O stretching vibration present in the EDTA as well as in $CaCO_3$ and confirms the contaminant iron adsorption on these groups.
3) The peak at 1383 cm^{-1} (C-H stretching vibration) has disappeared and the peak at 1107 cm^{-1} (C-O or C-O-C) shifted to 1114 cm^{-1} after treatment. The above changes in the peaks of functional groups present in EDTA also reveal iron adsorption.

The characterisation studies thus divulge the involvement of iron oxide/hydroxide shell, EDTA and $CaCO_3$ in the iron sorption process. The large specific surface area and strong unbalanced surface energy of nZVI make them highly tunable for various surface modifications leading to development of promising adsorbents. $CaC0_3$-nZVI formed by effective encapsulation possessed increased stability and exhibited synergy which contributed to the high removal efficiency of iron.

Adsorption isotherm modelling

The Langmuir, Freundlich and adsorption isotherms of surface modified nZVI were investigated by the adsorption data for varying initial concentration. The linearized equations of these models are given in Eqs. (1)-(3), respectively.

$$\frac{1}{q_e} = \frac{1}{q_m} + \frac{1}{q_m k_L} X \frac{1}{C_e} \text{Eq. (1)}$$

$$\log q_e = \log k_f + \frac{1}{n} \log C_e \text{Eq. (2)}$$

$$\ln q_e = \ln q_d - \bullet\bullet^2 \text{Eq. (3)}$$

Where C_e and q_e denotes iron concentration (mg/L) and sorption capacity (mg/g) at equilibrium, respectively. Langmuir constant, k_L, represents the adsorption free energy, and q_m defines maximum adsorption capacity (mg/g). k_f and n in Freundlich isotherm model represent the sorption capacity and adsorption intensity, respectively. The D-R isotherm constant q_d relates to maximum coverage (mg/g), and it is associated with mean free energy (E). Equations (4) and (5) are used to compute the parameter ε in the D-R isotherm and the mean free energy, respectively [10, 48].

$$e = RT \ln \left[1 + \frac{1}{C_e}\right] \text{Eq. (4)}$$

$$E = \frac{1}{\sqrt{2\bullet}} \text{Eq. (5)}$$

The isotherm plots are shown in Fig. 13, and the variables are provided in Table 1. As illustrated, the Freundlich model with a regression coefficient of 0.962 best describes iron removal by $CaCO_3$-nZVI. It demonstrates the possibilities

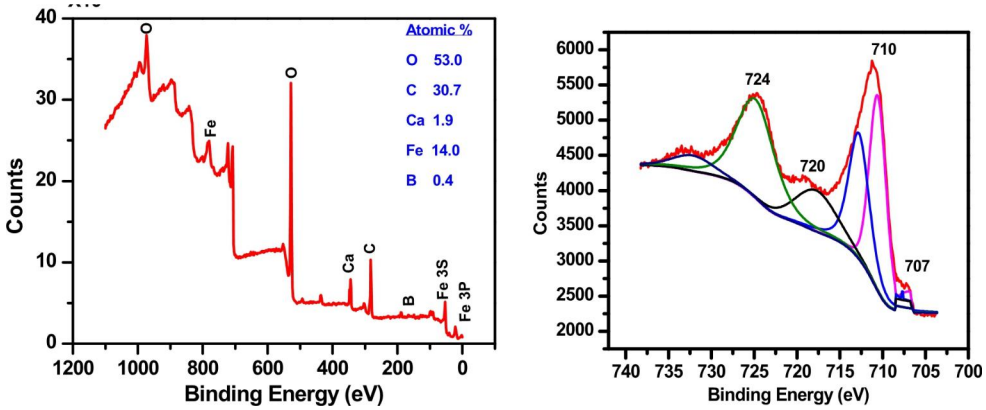

Fig. 10 **(a)** XPS surface spectrum and **(b)** Fe 2p spectrum of $CaCO_3$-nZVI after treatment

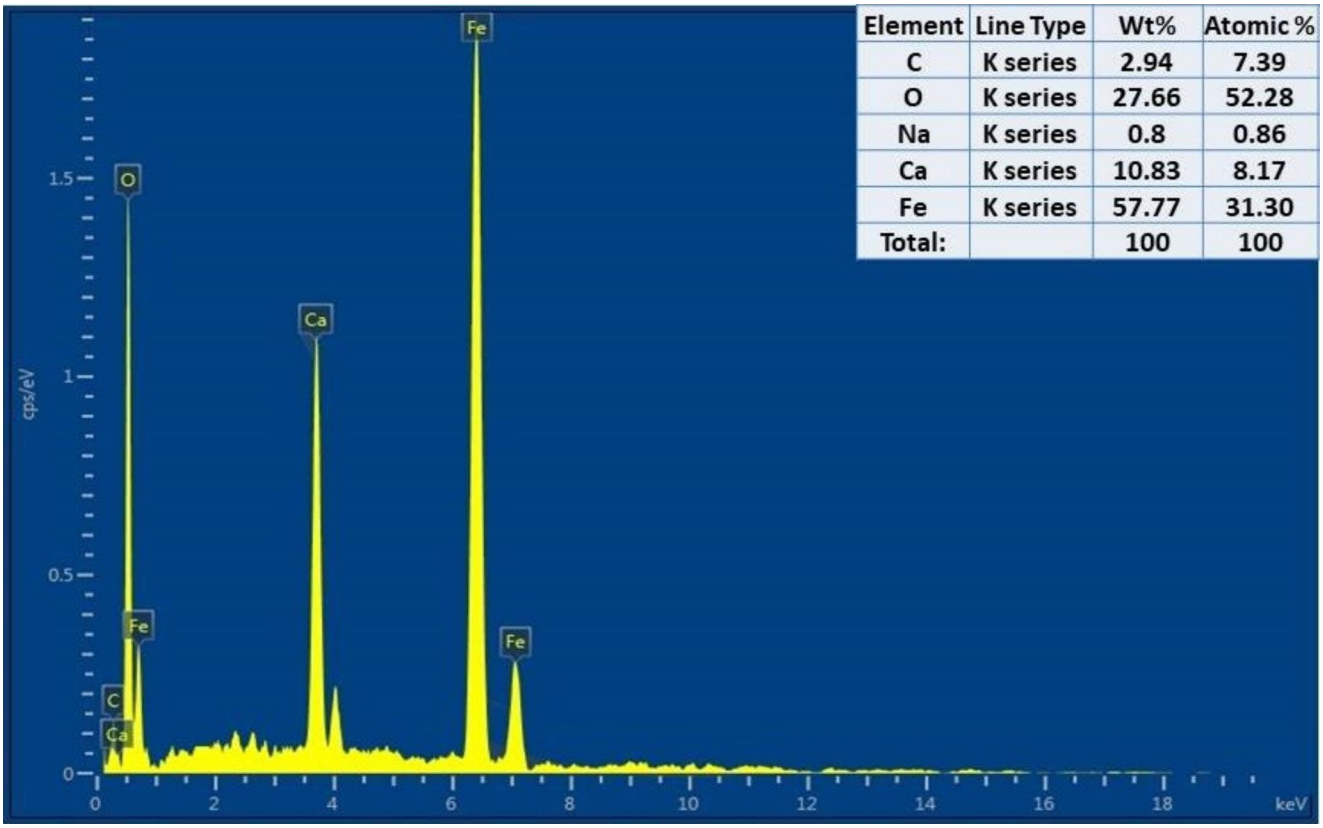

Fig. 11 EDX spectrum of $CaCO_3$-nZVI after treatment

of a heterogeneous surface, and that the available adsorption sites are distributed exponentially. According to this model theory, the sorption sites with high binding energy will be occupied first, and the active site energy would then decline exponentially as the sorption process progresses. The parameters of Freundlich isotherm, k_f and 1/n, represent sorption capacity factor and sorption intensity, respectively. The adsorption is irreversible when $1/n = 1$, while the adsorption is favourable when $1/n$ is greater than zero ($0 < 1/n < 1$), and it is unfavourable when $1/n > 1$. The obtained 1/n value for this study is 0.393 which indicates that the adsorption is favourable[48].

The regression coefficient for the Langmuir isotherm model is 0.952 and it indicates that this isotherm model may also be well adopted. The applicability of the Langmuir model can be evaluated by a dimensionless constant called separation factor, R_L and is expressed as:

$$R_L = \frac{1}{1 + k_L C_0} \text{Eq. (6)}$$

Where, C_0 is the influent iron content and k_L is the Langmuir constant. The separation factor for iron adsorption on $CaCO_3$-nZVI was in between 0 and 1, which further indicates favourable adsorption of iron [48].

The adsorption process on heterogeneous surfaces with Gaussian energy distribution are usually represented by the Dubinin-Radushkevich adsorption isotherm model. It's a pore-filling mechanism-based semi-empirical equation. The lower regression coefficient and calculated mean free energy, E (Table 1) ($E < 8$ kJ/mol), suggests that physical processes are in control of this adsorption [49].

Adsorption kinetics

To gain a better understanding of the kinetics of the process, the iron adsorption on $CaCO_3$- nZVI was investigated at various contact times. The iron solution, which had an initial concentration of 0.5 mg/L, was agitated with modified nZVI for 1 to 24 h. Pseudo-first order and pseudo-second order models were used to describe the kinetics. These models are described by the equations below:

$$.\ln (q_e - q_t) = \ln q_e - k_1 t \text{Eq. (7)}$$

$$\frac{t}{q_t} = \frac{1}{k_2 {q_e}^2} + \frac{1}{q_e} t \text{Eq. (8)}$$

Where adsorbed iron amount at equilibrium and at time t are represented by q_e and q_t, respectively. k_1 and k_2 are the

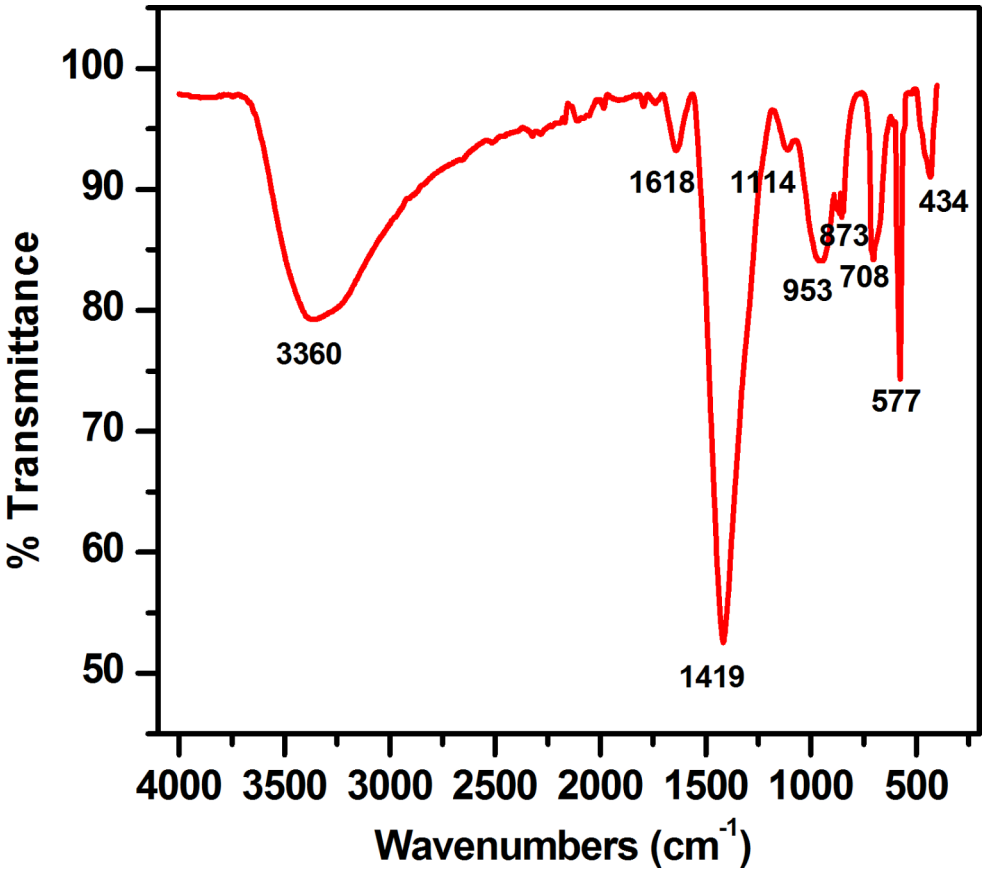

Fig. 12 FTIR spectrum of $CaCO_3$-nZVI after treatment

Table 1 Iron adsorption isotherm parameters for $CaCO_3$- nZVI

Langmuir isotherm			Freundlich isotherm			D-R isotherm			
q_m (mg/g)	k_L (L/mg)	R^2	k_f (mg/g)(L/mg)$^{1/n}$	n	R^2	q_d (mg/g)	β	E (kJ/mol)	R^2
7.64	18.44	0.952	9.91	2.545	0.961	8.26	2×10^{-8}	5	0.912

notations used to represent pseudo fist order and pseudo second order constants, respectively.

The Chi-square (χ^2) test and the regression coefficient (R^2) are used to assess the quality of kinetic model fit. The deviation between the model and experimental data can be calculated by Chi-square and its mathematical form is expressed as [50]:

$$\chi^2 = \sum \frac{[q_{e,exp} - q_{e,cal}]^2}{q_{e,cal}} \text{Eq. (9)}$$

Where sorption capacity of nanoparticle at equilibrium from experimental andmodel data are represented by $q_{e,exp}$ and $q_{e,cal}$, respectively.

The kinetic models in Fig. 14, as well as the values mentioned in Table 2, indicate that the iron sorption process of $CaCO_3$-nZVI was regulated by a pseudo-second-order reaction mechanism. The maximum adsorption capacity calculated using a pseudo-second-order kinetics is extremely close to the experimental value and χ^2 value for this model is very low. These findings suggest that the rate of adsorption is decided by adsorption capacity rather than influent iron concentration [51].

Comparison of different sorbents for iron removal

An adsorbent can be considered to be highly suitable when the following requirements are met, such as, (a) adsorption capacity (b) raw material abundance and (c) low cost. In this context, $CaCO_3$-nZVI can be considered to be a better adsorbent for iron removal in comparison to those reported in previous studies (Table 3) $CaCO_3$-nZVI outperformed both traditional sorbents and nano materials in iron removal. Moreover, the cost of the adsorbent is ₹150/kg which is less than conventional sorbents (activated carbon =₹200/kg). In comparison to study conducted in wastewater using a nano composite of carbon nanotubes (CNT) and nano iron oxide, the iron removal efficacy obtained in the present study is found to be low. However, as Fe_3O_4/CNT nano composite is toxic and expensive, its application is limited.

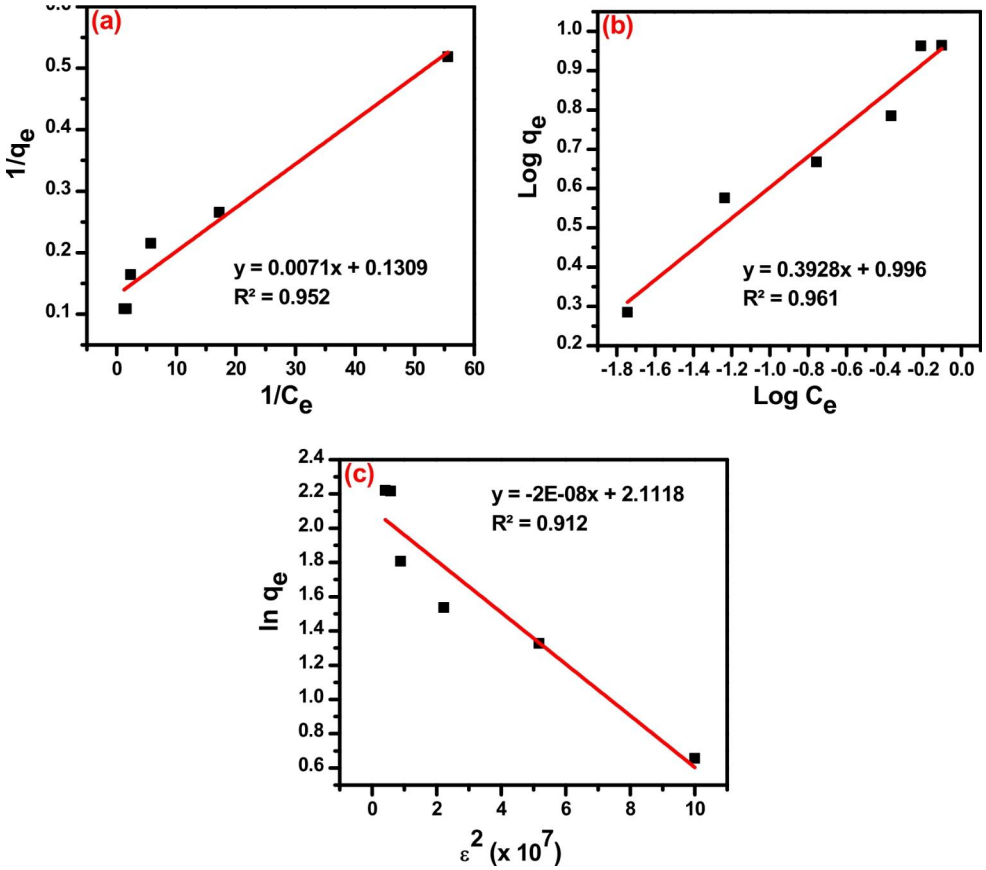

Fig. 13 Isotherm plots for iron adsorption on $CaCO_3$- nZVI: **(a)** Langmuir isotherm **(b)** Freundlich isotherm **(c)** D-R isotherm

Table 2 iron adsorption kinetic parameters for $CaCO_3$-nZVI

$q_{e,exp\ (mg/g)}$	Pseudo-first-order kinetics			Pseudo-second-order kinetics		
	$k_1\ (h^{-1})$	$q_{e,cal\ (mg/g)}$	R^2	$k_2\ (h^{-1})$	$q_{e,cal\ (mg/g)}$	R^2
3.96	0.327	0.982	0.435	0.168	4.26	0.988
χ^2	1.882			0.705		

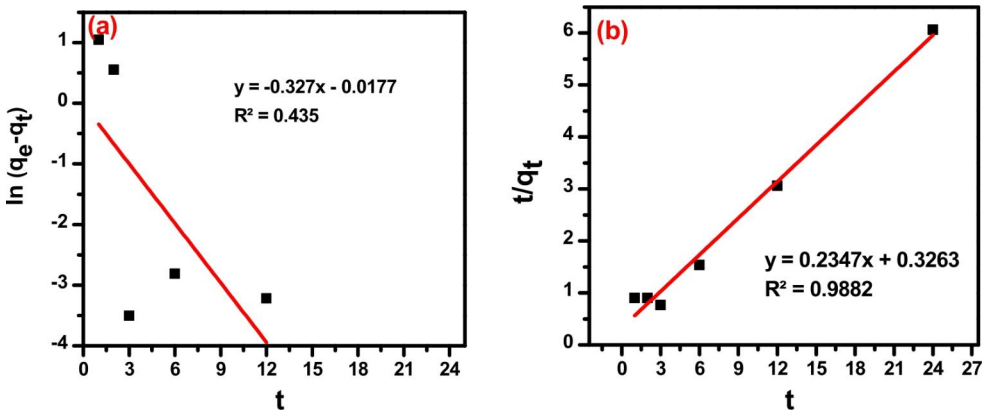

Fig. 14 **(a)** pseudo-first-order kinetic model **(b)** pseudo-second-order kinetic model

Conclusion

The prevention of aggregation behaviour as well as excellent iron removal performance was achieved through the surface modification of nZVI using $CaCO_3$. The TEM and SEM images as well as increment in BET surface area show the surface modification of nZVI favourable for enhanced adsorption. EDX, XRD, FTIR and XPS spectra revealed the elemental and functional characteristics of modified nanoparticle. Ratio of $CaCO_3$ to Fe in surface modification was found to affect the iron removal efficiency. Furthermore, the iron removal efficiency of $CaCO_3$-nZVI was

Table 3 Comparison of different sorbents for iron removal

Treatment unit	Type of water	Influent concentration (mg/L)	Effluent concentration (mg/L)	Removal efficiency (%)	Adsorption capacity (mg/g)	Reference
Activated Carbon	Tube well	5	0.84	83.2	-	Ismail et al., 2017
Groundnut shell activated carbon	Dam Water	3.11	0.31	90	-	Aji et al., 2015
Zeolite	Tube well	5	0.61	87.81	-	Ismail et al., 2017
Titanium oxide nanowire	Drinking water	2	0.4	79.77	-	Malhat and Youseff, 2014
MnO_2 modified nano hydroxyapatite	Ground water	0.68	0.15	77.6	0.606	Mamoon et al., 2019
Nano composite of CNT and nano iron oxide	Wastewater	10–20	0.11–0.22	98.97	200	Alimohammadi et al., 2017
$CaCO_3$- nZVI	Synthetic iron solution	0.5	0.018	96.4	7.64	Present study

gradually abated with increasing influent concentration (from 0.5 mg/L-10 mg/L), while an increase was found with increase in influent pH (from 3 to 12). $CaCO_3$-nZVI achieved 92.1-96.4% removal efficiency for influent iron concentration 0.5 to 10 mg/L at optimised operating conditions. The treatment process was well fitted with the Freundlich isotherm model and followed pseudo-second-order kinetics. The underlying mechanism of iron removal was investigated with the help of spectroscopic techniques. The increased iron percentage and emergence of new peaks corresponding to iron oxides in XRD and XPS reveals the uptake of iron as adsorption mechanism. The shifting of peaks in the FTIR spectrum and unchanged peak corresponding to Fe^0 in XRD as well as in XPS establish adsorption as iron removal mechanism. The remarkable iron removal efficiency and low cost of $CaCO_3$ encapsulated nZVI manifest that the sorbent has broad application prospects in environmental remediation.

Credit author statement.

JA: Conceptualization, methodology, formal analysis, investigation and writing – Original Draft; **VM**: Conceptualization, methodology, validation, project administration, funding acquisition, supervision, writing- review and editing; **VPR**: Conceptualization, methodology, validation, writing- review and editing, project administration and supervision; **PV**: Conceptualization, methodology, validation, writing- review and editing.

Acknowledgements The authors expressed their gratitude for the research facilities provided by the Government Engineering College Thrissur, Kerala. The services provided by the Sophisticated Test and Instrumentation Centre (STIC, CUSAT), CSIR-National Institute for Interdisciplinary Science and Technology (NIIST), Thiruvananthapuram and Centre for Materials for Electronics Technology (C-MET), Thrissur, for characterization studies are also greatly acknowledged.

Funding The All India Council for Technical Education (AICTE) funded this research under the NDF-RPS initiative for NDF research scholars.

Data Availability This manuscript contains all of the data generated or analysed during this research work.

Declarations

Declaration of competing interest This study has not been published and is not being considered for publication anywhere. We have no potential competing interests to disclose.

Ethics approval: Not applicable.

Consent to participate: Not applicable.

Consent to publish: Not Applicable.

References

1. Gehrke I, Geiser A, Somborn-Schulz A. Innovations in nanotechnology for water treatment. Nanotechnol Sci Appl. 2015;8:1–17.
2. Li XQ, Zhang WX. Sequestration of metal cations with zerovalent iron nanoparticles - A study with high resolution x-ray photoelectron spectroscopy (HR-XPS). J Phys Chem C. 2007;111:6939–46.
3. Gangadhar G, Maheshwari U, Gupta S. Application of Nanomaterials for the Removal of Pollutants from Effluent Streams. Nanosci &Nanotechnology-Asia. 2013;2:140–50.
4. Li S, Wang W, Liang F, Zhang WX. Heavy metal removal using nanoscale zero-valent iron (nZVI): Theory and application. J Hazard Mater [Internet]. Elsevier B.V.; 2017;322:163–71. Available from: https://doi.org/10.1016/j.jhazmat.2016.01.032.
5. Tosco T, Petrangeli Papini M, Cruz Viggi C, Sethi R. Nanoscale zerovalent iron particles for groundwater remediation: A review. J Clean Prod [Internet]. Elsevier Ltd; 2014;77:10–21. Available from: https://doi.org/10.1016/j.jclepro.2013.12.026.
6. Khatri N, Tyagi S, Rawtani D. Recent strategies for the removal of iron from water: A review. J Water Process Eng [Internet]. Elsevier; 2017;19:291–304. Available from: https://doi.org/10.1016/j.jwpe.2017.08.015.
7. Jismy A, Meera V, RaphaelVinod P. Comparative study on iron removal using chemically and greenly synthesised zero-valent iron nanoparticles. IOP Conf Ser Mater Sci Eng. 2021;1114:012082.
8. Antony J, Meera V, Raphael VP. Investigations on the capacity and mechanism of iron uptake by nano zero-valent iron particles. Bull Mater Sci. Indian Academy of Sciences; 2021;44–55. Available from: https://doi.org/10.1007/s12034-020-02274-5.
9. Ghosh GC, Khan MJH, Chakraborty TK, Zaman S, Kabir AHME, Tanaka H. Human health risk assessment of elevated and variable

iron and manganese intake with arsenic-safe groundwater in Jashore, Bangladesh. Sci Rep [Internet]. Springer US; 2020;10:1–9. Available from: https://doi.org/10.1038/s41598-020-62187-5.
10. Alimohammadi V, Sedighi M, Jabbari E. Experimental study on efficient removal of total iron from wastewater using magnetic-modified multi-walled carbon nanotubes. Ecol Eng Elsevier B V. 2017;102:90–7.
11. Kumar V, Bharti PK, Talwar M, Tyagi AK, Kumar P. Studies on high iron content in water resources of Moradabad district (UP), India. Water Sci [Internet]. National Water Research Center; 2017;31:44–51. Available from: https://doi.org/10.1016/j.wsj.2017.02.003.
12. Karakochuk CD, Murphy HM, Whitfield KC, Barr SI, Vercauteren SM, Talukder A, et al. Elevated levels of iron in groundwater in Prey Veng province in Cambodia: A possible factor contributing to high iron stores in women. J Water Health. 2015;13:575–86.
13. Willcomb GE. Iron and Manganese in Water. J Am Water Works Assoc. 2019;28:1896–909.
14. Hossain D, Islam M, Sultana N, Tusher T. Assessment of Iron Contamination in Groundwater at Tangail Municipality, Bangladesh. J Environ Sci Nat Resour. 2015;6:117–21.
15. Hindu T. Heavy metals contaminating India's rivers. hindu 2019 [Internet]. 2019 Dec 12; Available from: https://www.thehindu.com/news/national/heavy-metals-contaminating-indias-rivers/article30279681.ece.
16. Hindu T. High levels of iron found in water sources. 2015. https://www.thehindu.com/news/cities/Kochi/high-levels-of-iron-found-in-water-sources/article6877002.ece.
17. Pasinszki T, Krebsz M. Synthesis and application of zero-valent iron nanoparticles in water treatment, environmental remediation, catalysis, and their biological effects. Nanomaterials. 2020;10(5):917.
18. Tang H, Wang J, Zhang S, Pang H, Wang X, Chen Z, et al. Recent advances in nanoscale zero-valent iron-based materials: Characteristics, environmental remediation and challenges. J Clean Prod [Internet]. Elsevier Ltd; 2021;319:128641. Available from: https://doi.org/10.1016/j.jclepro.2021.128641.
19. Sun YP, Li X, qin, Cao J, Zhang W, xian, Wang HP. Characterization of zero-valent iron nanoparticles. Adv Colloid Interface Sci. 2006;120:47–56.
20. Cundy AB, Hopkinson L, Whitby RLD. Use of iron-based technologies in contaminated land and groundwater remediation: A review. Sci Total Environ [Internet]. Elsevier B.V.; 2008;400:42–51. Available from: https://doi.org/10.1016/j.scitotenv.2008.07.002.
21. Oprčkal P, Mladenovič A, Vidmar J, Mauko Pranjić A, Milačič R, Ščančar J. Critical evaluation of the use of different nanoscale zero-valent iron particles for the treatment of effluent water from a small biological wastewater treatment plant. Chem Eng J. 2017;321:20–30.
22. Zhang X, Lin S, Lu XQ, Chen ZL. Removal of Pb(II) from water using synthesized kaolin supported nanoscale zero-valent iron. Chem Eng J [Internet]. Elsevier B.V.; 2010;163:243–8. Available from: https://doi.org/10.1016/j.cej.2010.07.056.
23. Xi Y, Megharaj M, Naidu R. Dispersion of zerovalent iron nanoparticles onto bentonites and use of these catalysts for orange II decolourisation. Appl Clay Sci [Internet]. Elsevier B.V.; 2011;53:716–22. Available from: https://doi.org/10.1016/j.clay.2011.06.010.
24. Shi L, Zhang X, Chen Z. Removal of Chromium (VI) from wastewater using bentonite-supported nanoscale zero-valent iron. Water Res [Internet]. Elsevier Ltd; 2011;45:886–92. Available from: https://doi.org/10.1016/j.watres.2010.09.025.
25. Bhowmick S, Chakraborty S, Mondal P, Van Renterghem W, Van den Berghe S, Roman-Ross G, et al. Montmorillonite-supported nanoscale zero-valent iron for removal of arsenic from aqueous solution: Kinetics and mechanism. Chem Eng J [Internet]. Elsevier B.V.; 2014;243:14–23. Available from: https://doi.org/10.1016/j.cej.2013.12.049.
26. Ezzatahmadi N, Ayoko GA, Millar GJ, Speight R, Yan C, Li J, et al. Clay-supported nanoscale zero-valent iron composite materials for the remediation of contaminated aqueous solutions: A review. Chem Eng J [Internet]. Elsevier B.V.; 2017;312:336–50. Available from: https://doi.org/10.1016/j.cej.2016.11.154.
27. Dong H, Lo IMC. Influence of calcium ions on the colloidal stability of surface-modified nano zero-valent iron in the absence or presence of humic acid. Water Res [Internet]. Elsevier Ltd; 2013;47:2489–96. Available from: https://doi.org/10.1016/j.watres.2013.02.022.
28. Saha AK, Sinha A, Pasupuleti S. Modification, characterization and investigations of key factors controlling the transport of modified nano zero-valent iron (nZVI) in porous media. Environ Technol (United Kingdom) Taylor & Francis. 2019;40:1543–56.
29. Dong H, Zeng G, Zhang C, Liang J, Ahmad K, Xu P, et al. Interaction between Cu2 + and different types of surface-modified nanoscale zero-valent iron during their transport in porous media. J Environ Sci (China) [Internet]. Elsevier B.V.; 2015;32:180–8. Available from: https://doi.org/10.1016/j.jes.2014.09.043.
30. Huang DL, Chen GM, Zeng GM, Xu P, Yan M, Lai C, et al. Synthesis and Application of Modified Zero-Valent Iron Nanoparticles for Removal of Hexavalent Chromium from Wastewater. Water Air Soil Pollut. 2015;226.
31. Dong H, He Q, Zeng G, Tang L, Zhang C, Xie Y, et al. Chromate removal by surface-modified nanoscale zero-valent iron: Effect of different surface coatings and water chemistry. J Colloid Interface Sci. 2016;471:7–13.
32. Fatisson J, Ghoshal S, Tufenkji N. Deposition of carboxymethylcellulose-coated zero-valent iron nanoparticles onto silica: Roles of solution chemistry and organic molecules. Langmuir. 2010;26:12832–40.
33. Mosaferi M, Nemati S, Khataee A, Nasseri S, Hashemi AA. Removal of arsenic (III, V) from aqueous solution by nanoscale zero-valent iron stabilized with Starch and Carboxymethyl cellulose. J Environ Heal Sci Eng. 2014;12:1–11.
34. You W, Weng Y, Wang X, Zhuang Z, Yu Y. Synthesis and Adsorption Properties of Hierarchically Ordered Nanostructures Derived from Porous CaO Network. ACS Appl Mater Interfaces. 2016;8:33656–65.
35. Zhang X, Shi D, Li X, Zhang Y, Wang J, Fan J. Nanoscale dispersing of zero-valent iron on CaCO3 and their significant synergistic effect in high performance removal of lead. Chemosphere [Internet]. Elsevier Ltd; 2019;224:390–7. Available from: https://doi.org/10.1016/j.chemosphere.2019.02.139.
36. Ma X, Li L, Yang L, Su C, Wang K, Yuan S, et al. Adsorption of heavy metal ions using hierarchical CaCO 3-maltose meso/macroporous hybrid materials: Adsorption isotherms and kinetic studies. J Hazard Mater [Internet]. Elsevier B.V.; 2012;209–210:467–77. Available from: https://doi.org/10.1016/j.jhazmat.2012.01.054.
37. Ahmad K, Bhatti IA, Muneer M, Iqbal M, Iqbal Z. Removal of heavy metals (Zn, Cr, Pb, Cd, Cu and Fe) in aqueous media by calcium carbonate as an adsorbent. 2012;2:48–53.
38. Jacob JJ, Varalakshmi R, Gargi S, Jayasri MA, Suthindhiran K. Removal of Cr (III) and Ni (II) from tannery effluent using calcium carbonate coated bacterial magnetosomes. npj Clean Water [Internet]. Springer US; 2018;1. Available from: https://doi.org/10.1038/s41545-018-0001-2.
39. Sdiri A, Higashi T. Simultaneous removal of heavy metals from aqueous solution by natural limestones. Appl Water Sci. 2013;3:29–39.
40. Cheng Y, Dong H, Hao T. CaCO3 coated nanoscale zero-valent iron (nZVI) for the removal of chromium(VI) in aqueous solution.

Sep Purif Technol [Internet]. Elsevier B.V.; 2020;117967. Available from: https://doi.org/10.1016/j.seppur.2020.117967.
41. Bao T, Damtie MM, Hosseinzadeh A, Frost RL, Yu ZM, Jin J, et al. Catalytic degradation of P-chlorophenol by muscovite-supported nano zero valent iron composite: Synthesis, characterization, and mechanism studies. Appl Clay Sci. 2020;195.
42. Subin MP, Anitha CT, Sidhimol PD. The Study of Water Quality of Tripunithura, a City Suburb of Ernakulam District in Kerala, India. 2011;10.
43. Yang F, Zhang S, Sun Y, Cheng K, Li J, Tsang DCW. Fabrication and characterization of hydrophilic corn stalk biochar-supported nanoscale zero-valent iron composites for efficient metal removal. Bioresour Technol [Internet]. Elsevier Ltd; 2018;265:490–7. Available from: https://doi.org/10.1016/j.biortech.2018.06.029.
44. Wang B, Yang X, Wang L, Li G, Li Y. Facile preparation of CaCO3 with diversified patterns modulated by N-[(2-hydroxyl)-propyl-3-trimethylammonium] chitosan chloride. Powder Technol [Internet]. Elsevier B.V.; 2016;299:51–61. Available from: https://doi.org/10.1016/j.powtec.2016.05.036.
45. Linggawati A. Preparation and Characterization of Calcium Oxide Heterogeneous Catalyst Derived from Anadara Granosa Shell for Biodiesel Synthesis. KnE Eng. 2016;1:0–8.
46. Galván-Ruiz M, Hernández J, Baños L, Noriega-Montes J, Rodríguez-García ME. Characterization of Calcium Carbonate, Calcium Oxide, and Calcium Hydroxide as Starting Point to the Improvement of Lime for Their Use in Construction. J Mater Civ Eng. 2009;21:694–8.
47. Ismail A, Harmuni H, Mohd RRMAZ. Removal of iron and manganese using granular activated carbon and zeolite in artificial barrier of riverbank filtration. 2017;1842:020056.
48. Wang J, Guo X. Adsorption isotherm models: Classification, physical meaning, application and solving method. Chemosphere [Internet]. Elsevier Ltd; 2020;258:127279. Available from: https://doi.org/10.1016/j.chemosphere.2020.127279.
49. Hu Q, Zhang Z. Application of Dubinin–Radushkevich isotherm model at the solid/solution interface: A theoretical analysis. J Mol Liq [Internet]. Elsevier B.V; 2019;277:646–8. Available from: https://doi.org/10.1016/j.molliq.2019.01.005.
50. Boparai HK, Joseph M, Carroll DMO. Kinetics and thermodynamics of cadmium ion removal by adsorption onto nano zerovalent iron particles. J Hazard Mater [Internet]. Elsevier B.V.; 2011;186:458–65. Available from: https://doi.org/10.1016/j.jhazmat.2010.11.029.
51. Sasidharan AP, Raphael VM. VP. Performance of nanosilver/silver oxide in sorbing phosphate from synthetic greywater. SSRN Electron J. 2022;24–6.

Supplementary Information The online version contains supplementary material available at https://doi.org/10.1007/s40201-022-00831-0.